JET–P(98)52

G A Cottrell et al

Ion Cyclotron Heating of JET D–D and D–T Optimised Shear Plasmas

JET–P(98)52

Ion Cyclotron Heating of JET D–D and D–T Optimised Shear Plasmas

G A Cottrell, Y Baranov, D Bartlett, C D Challis, A Ekedahl[1], L–G Eriksson, C Gormezano, G T A Huysmans, X Litaudon[2], M Mantsinen[3], D O'Brien, V Parail, F Rochard[2], G J Sadler, P Schild, A C C Sips, F X Söldner, D F H Start, B J D Tubbing, D J Ward, M von Hellermann, W P Zwingmann.

JET Joint Undertaking, Abingdon, Oxfordshire, OX14 3EA,
[1]Also at: Chalmers University of Technology, Gothenburg, Sweden.
[2]Permanent address: CEA Cadarache, France.
[3]Also at: Helsinki University of Technology, Association Euratom-TEKES, Espoo, Finland.

Preprint of a Paper accepted for publication in Nuclear Fusion

December 1998

ABSTRACT

This paper discusses the unique roles played by Ion Cyclotron Resonance Heating (ICRH) in the preparation, formation and sustainment of internal transport barriers (ITBs) in high fusion performance JET optimised shear experiments using the Mk. II poloidal divertor. Together with Lower Hybrid Current Drive (LHCD), low power ICRH is applied during the early ramp-up phase of the plasma current, 'freezing in' a hollow or flat current density profile with $q(0)>1$. In combination with up to ~ 20 MW of Neutral Beam Injection (NBI), the ICRH power is stepped up to ~ 6 MW during the main low confinement (L-mode) heating phase. An ITB forms promptly after the power step, revealed by a region of reduced central energy transport and peaked profiles, with the ion thermal diffusivity falling to values close to the standard neo-classical level near the centre of both D-D and D-T plasmas. At the critical time of ITB formation, the plasma contains an energetic ICRF hydrogen minority ion population, contributing ~ 50% to the total plasma pressure and heating mainly electrons. As both the NBI population and the thermal ion pressure develop, a substantial part of the ICRF power is damped resonantly on core ions ($\omega = 2\ \omega_{cD} = 3\ \omega_{cT}$) contributing to the ion heating. In NBI step-down experiments, high performance has been sustained by maintaining central ICRH heating; analysis shows the efficiency of central ICRH ion heating to be comparable with that of NBI. The highest D-D fusion neutron rates ($R_{NT} = 5.6 \times 10^{16}\ s^{-1}$) yet achieved in JET plasmas have been produced by combining a low magnetic shear core with a high confinement (H-mode) edge. In D-T, a fusion triple product $n_i T_i \tau_E = (1.2 \pm 0.2) \times 10^{21}\ m^{-3}$ keVs was achieved with 7.2 MW of fusion power obtained in the L-mode and up to 8.2 MW of fusion power in the H-mode phase.

1. INTRODUCTION

A major focus of the programme to develop thermonuclear fusion power in tokamaks is the exploration of advanced regimes of operation, aiming to reduce energy losses from the plasma. Improvements in performance can be gained by optimising the kinetic pressure profile - increasing it up to the limit imposed by MHD stability. One well-known regime where improvements have already been made in tokamaks equipped with a magnetic poloidal divertor is the H-mode, where a thermal transport barrier forms in a narrow radial region just inside the magnetic separatrix. However, it has been found that the characteristically steep edge pressure gradient of the H-mode can destabilise edge-localised MHD modes (ELMs) and outer MHD modes which can limit steady-state fusion performance in the ELM-free regime. In addition, the central plasma pressure of an H-mode is limited by sawteeth as well as by other MHD activity, such as neo-classical tearing modes.

We note that the fusion core reactivity scales as approximately the square of the central ion pressure and the total reactivity scales as approximately the square of the global plasma stored energy. Alternative improved regimes are aimed at increasing the particle and energy confinement in the plasma core (by establishing an ion transport barrier). In a burning fusion

reactor the energetic fusion alpha-particles transfer most of their energy classically to the thermal electrons. A fraction of this energy is redistributed, by collisions, to the thermal ions which sustains their temperature and maintains the reaction. However electron conductive and convective losses also compete and so it is important to try and reduce these energy losses (by establishing an electron transport barrier) so that energy in the electron population is redistributed amongst the ions.

To improve central plasma performance, sawteeth can be avoided for some time by operating the tokamak with a value of the central safety factor, $q(0) > 1$, a regime that can be accessed by applying additional heating during the current rise phase. Improved central confinement and high performance have both been demonstrated on JET by central pellet fuelling of sawtooth-free discharges combined with intense central heating [1]. The central magnetic shear ($s = r/q(\mathrm{d}q/\mathrm{d}r)$) in these discharges was low and negative [2]. More recently, other large tokamaks (TFTR [3], DIII-D [4] and JT60 [5]) have explored neutral beam injection (NBI) heating during the current rise and all have demonstrated improvements in the central confinement and in fusion performance.

The use of ICRH, available on JET in addition to NBI, adds a second additional heating system which has been used to explore further the improved regimes. When high power combined ICRF and NBI heating was applied to JET tokamak plasmas during the early current rise phase (the optimised shear regime), the central plasma confinement is also observed to improve - this occurs when the magnetic shear in the central region is close to zero [6 - 9]. Transport analysis studies of JET optimised shear pure deuterium plasmas [10] show that the position and rate of expansion of the radius of the internal transport barriers of electron density, ion temperature, ion thermal diffusivity and momentum diffusivity correlate (within $\Delta\rho \sim 0.1$ in normalised radius) with the calculated position of the $q = 2$ surface in the plasma. Using D-T fuel, a fusion triple product $n_i T_i \tau_E = (1.2 \pm 0.2) \times 10^{21}$ m^{-3} keVs has been achieved with the generation of 7.2 MW of fusion power in the L-mode and up to 8.2 MW in the subsequent H-mode phase [11].

This paper is organised as follows. In Section 2, the role of ICRH is illustrated by comparing two high performance discharges with deuterium and deuterium-tritium fuel. In Section 3, we present results of analysis of the direct ion heating of ICRF in the core of the optimised shear plasma and an analysis of the sustainment of the internal transport barrier with ICRF heating during a step-down of the NBI power. Section 4 discusses the results and Section 5 summarises the conclusions. A description of the data analysis and physics models used appears in the Appendix, placing emphasis on a description of the ICRF modelling. A list of the JET pulses analysed in this paper is given in Table I.

TABLE I. List of JET discharges analysed in this paper

Pulse	**Gas**	**P_{RF}**	**P_{NBI}**	**Comments**
40210 (A1)	DD	6.1 MW	17.1 MW → 10.2 MW	NBI power step-down during L-mode ITB
40214 (C1)	DD		18.2 MW	NBI-only ITB
40215 (B1)	DD	6.0 MW → 2 MW	17.1 MW	ICRF power step-down during L-mode ITB
40554 (A)	DD	6.0 MW	18.7 MW	Highest performance DD OS pulse. BT = 3.4 T
42746 (B)	DT	6.1 MW	(D) 9.2 MW (T) 7.2 MW	Highest performance DT OS pulse. P_{fus} = 8.2 MW in H-mode phase. BT = 3.4 T.
42940	DT	6.1 MW	(D) 11 MW (T) 10.6 MW	High performance DT OS pulse. P_{fus} = 7.2 MW in L-mode phase. BT = 3.8 T.

2. THE ROLE OF ICRH IN OPTIMISED SHEAR DISCHARGES

2.1 Typical Optimised Shear Discharges

There are two basic phases in the production of JET high performance optimised shear discharges: a preheating phase and a main heating phase. In the preheating phase, a low density ($n_e(0) \leq 1.5 \times 10^{19}$ m^{-3}) target plasma with a flat or hollow current density $j(r)$ profile with $q(0) > 1$ is produced by carefully controlled preheating during the early current rise. This is followed by a main heating phase in which the core of the plasma is heated strongly using combined ICRF and NBI additional heating. Experimentally it has been found that, provided the $j(r)$ profile is suitably established, a transition to a state of improved core confinement (reduced turbulence and losses in the central part of the plasma) can spontaneously occur in the second phase. This is known as the internal transport barrier. The clearest signature of the presence of an internal transport barrier is a sharp change in the radial gradient of the ion temperature, T_i (the 'footpoint' of the internal transport barrier). To illustrate the formation and evolution of a typical L-mode internal transport barrier, we show a contour plot of $\nabla^2 T_i$ for a deuterium-tritium pulse (No. 42940, Fig. 1). The arête, or ridge, in this contour plot tracks the evolution of the position of the footpoint of the region of improved confinement which expands with a radial velocity of about 0.5 m s^{-1}.

ICRH plays two distinct and important roles in both the preheating and the main heating phases. First, during the phase of preheating during the current rise, low ICRH power (typically ~ 1 MW) is applied in the minority - (H)D or (H)DT scheme - at the fundamental hydrogen ion cyclotron resonance in the plasma centre. In this early phase of the plasma evolution, the

thermal ion pressure is relatively small and most of the the RF power is coupled to hydrogen minority ions. When the concentration of minority ions is at the level of a few percent, and with typical plasma conditions, electron heating via collisional power transfer from the ICRH minority tail is efficient. Thus the application of ICRH in the early phase reduces the parallel plasma resistivity and provides a method to control and delay the inward diffusion of the plasma current, allowing the required flat or hollow current density j(r) profile with central safety factor $q(0) > 1$ to be maintained. ICRH also has the advantage of heating in narrow, pre-selected deposition region without the associated injection of particles into the plasma centre as is the case with NBI preheating. In practice, we have found that this feature is useful since we have found, by experiment, that provided that a low density target plasma is created, internal transport barriers will form promptly and reliably after the application of the main heating waveform. In the case that the target plasma density is too high, then an early H-mode transition is likely to be triggered which can preclude the formation of a strong internal transport barrier.

Once the plasma current has diffused sufficiently to give the required low central magnetic shear target q(r) profile with $1 < q(0) < 2$, the main heating waveforms are applied, consist-

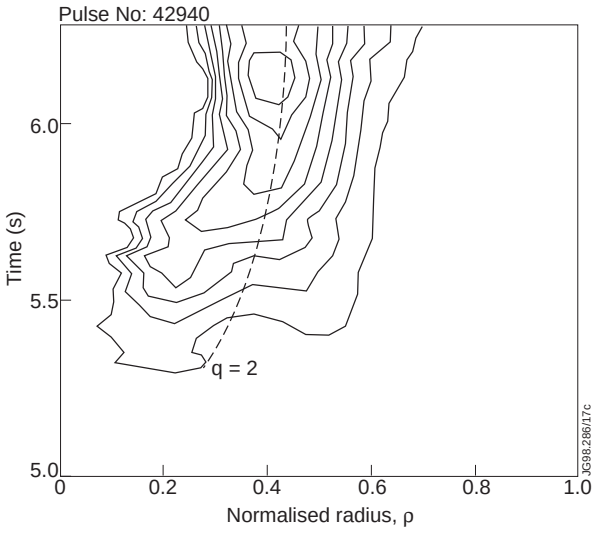

Fig 1. Evolution of the position of the 'footpoint' of the internal transport barrier revealed as contours of $\nabla^2 T_i$ in the time-normalised radius plane for a toroidal field B_T = 3.8 T deuterium-tritium pulse (No. 42940) which produced a fusion power of 7.2 MW in the L-mode phase.

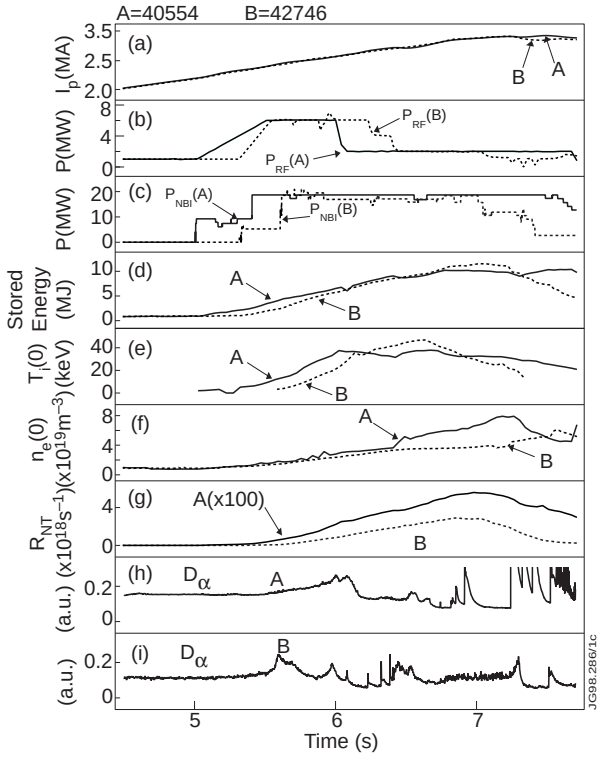

Fig 2. Evolution of plasma parameters in two JET high performance optimised shear discharges with toroidal field B_T = 3.4 T; these are: pure deuterium Pulse "A" (No. 40554) and deuterium-tritium Pulse "B" (No. 42746). Traces: (a) plasma current, I_P; (b) NBI and ICRF auxiliary heating powers; (c) diamagnetic energy content, W_{dia} ; (d) central ion temperatures, $T_i(0)$; (e) central electron densities, $n_e(0)$; (f) total neutron emission rates, R_{NT}; (g) D_α emissivity trace (pulse A) and (g) D_α emissivity trace (pulse B).

ing typically of 15 MW-20 MW of NBI power combined with 6 MW of ICRH power. Experimentally we have found that the minimum NBI power needed to trigger an internal transport barrier reliably is around the 15 MW level; however we have observed short-lived L-mode internal transport barriers with only 12 MW of NBI in both pure deuterium and deuterium-tritium plasmas.

Comparative examples of the two highest performing JET optimised shear discharges obtained during the Mk. II poloidal divertor campaign are shown in Fig. 2 with parameters given in Table II. These are: pure deuterium Pulse "A" (No. 40554) and deuterium-tritium Pulse "B" (No. 42746). Pulse A was the model for pulse B. In each case, the early preheating phase included a short pulse of 1 MW of LHCD power applied from time t = 0.4 s - 1.2 s. This was followed by 1 MW of ICRH preheating power from t = 2.9 s - 5.0 s (case A) and from t = 3.2 s - 5.3 s (case B), until the start of the main heating phase.

TABLE II. Plasma Parameters for two high performance JET optimised shear pulses: a pure Deuterium case (A), (Pulse No. 40554), and a Deuterium-Tritium case (B), (Pulse No. 42746) at the peak fusion performance times.

Pulse	40554 (Pulse A)	42746 (Pulse B)
Time	7.0 s	6.86 s
Toroidal Field BT	3.4 Tesla	3.4 Tesla
Plasma Current IP	3.2 MA	3.2 MA
NBI D-beam Power	18.6 MW	9.2 MW
NBI T-beam Power	0	7.2 MW
ICRH Power	2.0 MW	2.0 MW
Diamagnetic Stored Energy	10.1 MJ	11.2 MJ
Central Electron Density $n_e(0)$	6.2×10^{19} m^{-3}	3.9×10^{19} m^{-3}
Central D ion Density $n_D(0)$	4.9×10^{19} m^{-3}	2.1×10^{19} m^{-3}
Central T ion Density $n_T(0)$	0	1.1×10^{19} m^{-3}
Central Electron Temperature $T_e(0)$	12.5 keV	12.5 keV
Central Ion Temperature $T_i(0)$	24 keV	33 keV
Total Neutron Emission R_{NT}	5.6×10^{16} s^{-1}	2.9×10^{18} s^{-1}

A feature of the use of tritium fuelling in JET divertor discharges is a reduction of the H-mode power threshold [12]. Since our objective in these experiments was to establish an internal transport barrier before the discharge made a transition into the H-mode, it was necessary to modify the timings of the heating waveforms in order to avoid the early formation of the H-mode. In pulse B, the first NBI step was delayed (starting at t = 5.4 s), was smaller (P_{NBI} = 5.3 MW) and the ICRH ramp steeper than in pulse A. In this pulse, at t = 5.0 s, a bank of near radially-directed neutral beams (P_{NBI} = 9.3 MW) was injected into the low density ($n_e(0) = 1.5 \times 10^{19}$ m^{-3}) target plasma and the ramp-up from 1 MW to 6 MW of ICRH power started. As both plasma

density and current increased, a bank of near tangentially-directed neutral beams was added giving a total NBI power of 18.7 MW combined with 6 MW of ICRH at t = 5.4 s. About 0.2 s later, there is a spontaneous transition to a state of improved central confinement - the formation of an internal transport barrier. The confinement improvement starts in the plasma centre and then propagates outwards, reaching a normalised radius of $\rho \sim 0.55$ at t = 6.4 s. Both the plasma density and current continue to increase with the current reaching its maximum flat-top value of 3.3 MA at t = 7.2 s. At t = 6.95 s, there is an L-mode to H-mode transition - shown by the rapid decrease in D_α emission - indicating the formation of an ELM-free H-mode.

A difference between the two pulses is the behaviour of the electron density; in pulse A, at t = 7.3 s, the central value reaches a maximum value of $n_e(0) = 7.0 \times 10^{19}$ m^{-3} whereas in pulse B it reaches $n_e(0) = 5.5 \times 10^{19}$ m^{-3} at t = 7.5 s. This difference can be related to the difference in the total particle refuelling rates when eight (out of sixteen) of the NBI plasma sources were converted from deuterium to tritium in pulse B. The total NBI particle input to the plasma is, in D-D pulse A, 36 % higher than in D-T pulse B. The central ion temperature in pulse B reaches a maximum value of $T_i(0)$ = 36 keV, whereas in pulse A it is $T_i(0)$ = 25 keV at t = 6.6 s. At this time the central thermal pressures in the two discharges are almost equal $p(0) \approx 4.4 \times 10^5$ Pa. The Shafranov shift is relatively large in the high performance phase, increasing from 0.07 m at the end of the low-β preheating phase to typically 0.24 m at t = 6.6 s in both pulses.

The evolution of the ion temperature in pulse A is shown in Fig. 3 and the plasma pressure profiles for pulses A and B in Figs. 4(a) and 4(b). The peaking of plasma profiles increases progressively during the L-mode phase. Figures 5(a) and 5(b) show the evolution of the electron temperature profiles, $T_e(R)$, for the two pulses. From the change in ∇T_e at approximately 0.5 s after the application of the main heating, it can be seen that an electron internal transport barrier is formed during the ion heating regime [13]. The central plasma parameters remain high during the ELM-free H-mode phase, but the rate of rise of the total 2.5 MeV DD neutron emission rate in pulse A decreases at t = 6.8 s (reaching a peak value of $R_{NT} = 5.6 \times 10^{16}$ s^{-1} at t = 7.0 s). The rate of rise of the diamagnetic stored energy also decreases, near the time of the H-mode transition. By this time the central electron density reaches $n_e(0) = 6.2 \times 10^{19}$ m^{-3}; the central electron temperature is $T_e(0)$ = 12.5 keV and the central ion temperature remains at $T_i(0)$ = 24 keV.

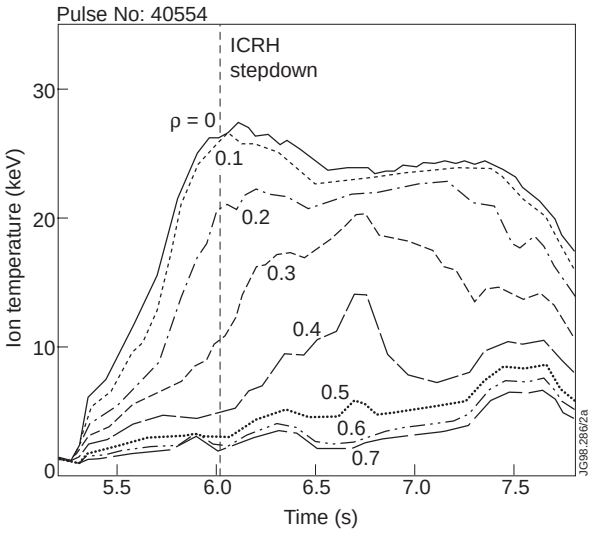

Fig 3. Evolution of the ion temperature at different normalised radii from charge-exchange recombination measurements for pulse A. The time of the ICRH power stepdown from 6 MW to 2 MW is indicated. Typical error bars are ± 1 keV.

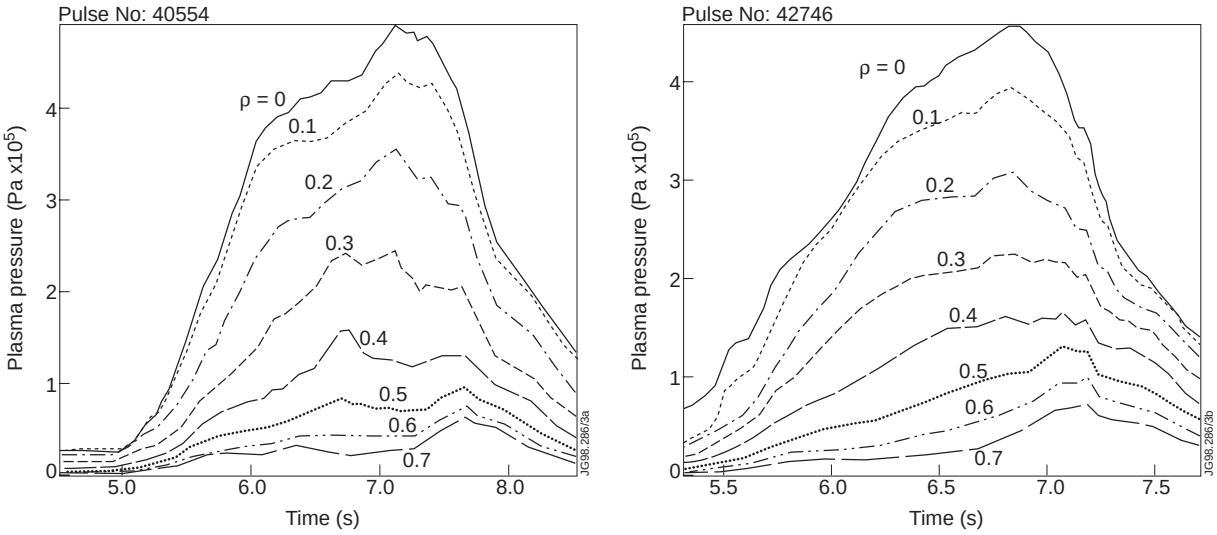

Fig. 4. Evolution of total plasma pressure at different normalised radii; (a) for pulse A; (b) for pulse B.

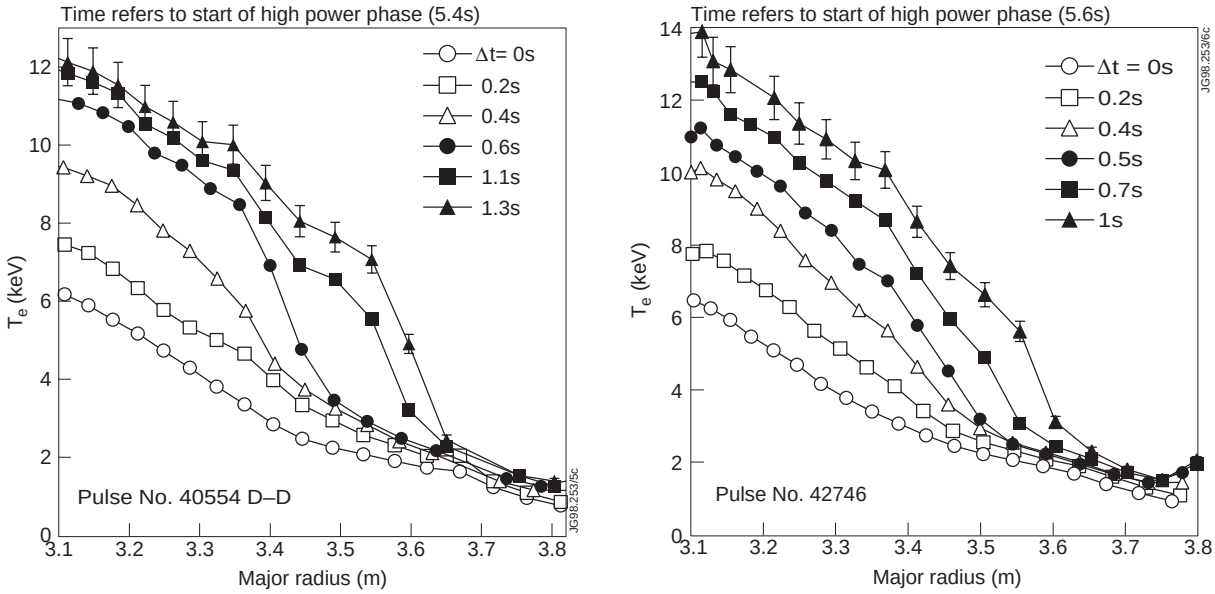

Fig. 5. Evolution of the electron temperature profiles; (a) for pulse A; (b) for pulse B.

2.2 Data Consistency

In the analysis presented here, we have made extensive use of the TRANSP and PION codes (see Appendix for details). To check the self-consistency of the various diagnostic data, local values of basic quantities such as density, temperature and effective plasma charge, Z_{eff}, were, input to the TRANSP model in the first instance. The model predicts a new, larger, set of data including both local and global quantities, including the total neutron emission rate and the total diamagnetic stored energy in the discharge which can be checked against independent measurements. The ability of a simulation to reproduce these data provides a measure of the self-consistency of the input data set. The aim of the modelling was therefore: first to validate the input diagnostic data self-consistently, then infer the underlying energy, momentum and particle transport coefficients that are consistent with the measured input data.

The primary input data to the TRANSP code are as follows. The bulk ion, minority ion and nominal impurity ion species are specified. Magnetic data used include the position of the plasma boundary, the total plasma current and toroidal field. We also input electron density profile data (from LIDAR measurements), ion temperature, effective plasma charge and toroidal rotation velocity (from charge-exchange recombination measurements during the time window when the relevant neutral beam injection sources are active). The total radiation loss, measured by a bolometer, is also included. The electron temperature (from electron cyclotron emission measurements) is input as a function of frequency and then mapped, self-consistently, on to the radial space co-ordinate using the TRANSP equilibrium solver.

This analysis was applied to a number of JET optimised shear discharges including the examples shown in Fig. 2. The TRANSP (model 1, see Appendix) calculated neutron rate for D-T pulse B (Fig. 6) lies within the measurement error bars (± 10 %), with thermonuclear neutron emission comprising approximately 50 % of the total, beam-thermal neutrons accounting for 46 % and the remainder arising from beam-beam reactions. In pulse A, thermonuclear reactions comprise up to 70% of the total neutron rate from the plasma; the increase over pulse B is due to the longer time duration of the L-mode phase and the higher level of plasma density. The computed diamagnetic energy content agrees well with measurement, lying within the estimated error band of ± 1 MJ (Fig. 7). In the early critical time window (between t = 5.5 s and 6.5 s) during which the internal transport barrier is formed, the dominant component of the diamagnetic stored energy content comes from energetic ions. Only later, once the internal transport barrier has become well established (t > 6.5 s), does the thermal energy content dominate, reaching a value of 60 % at t = 6.84 s, and a maximum of 71 % of the total at t = 7.1 s. The profiles of the energy densities of the various plasma components for deuterium-tritium pulse No. 42940 are shown in Fig. 8 at t = 5.5 s, approximately the time of the formation of the internal transport barrier. The dominance of the perpendicular components of fast ICRH and NBI ion energy densities over the thermal energy density component within radius $\rho \approx 0.5$ can clearly be seen. The ICRH hydrogen minority ions constitute about half of the total; from the TRANSP model 1 analysis these minority ions have calculated average particle energies in the range of a few MeV in the core of the plasma. These ICRH ions heat thermal electrons effectively but, at this early stage in the evolution, relatively little RF power is coupled to the thermal ions.

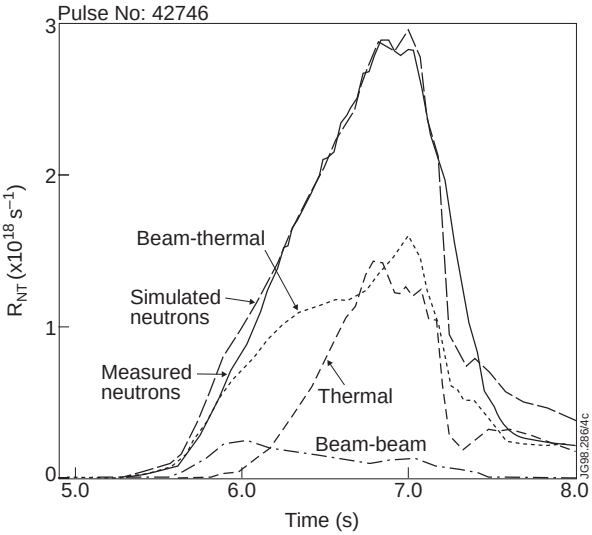

Fig. 6. TRANSP code neutron emission modelling for deuterium-tritium pulse B, comparing the measured and simulated total neutron emission rates. The simulated total neutron emission rate is the sum of the thermal-thermal, beam-thermal and beam-beam rates.

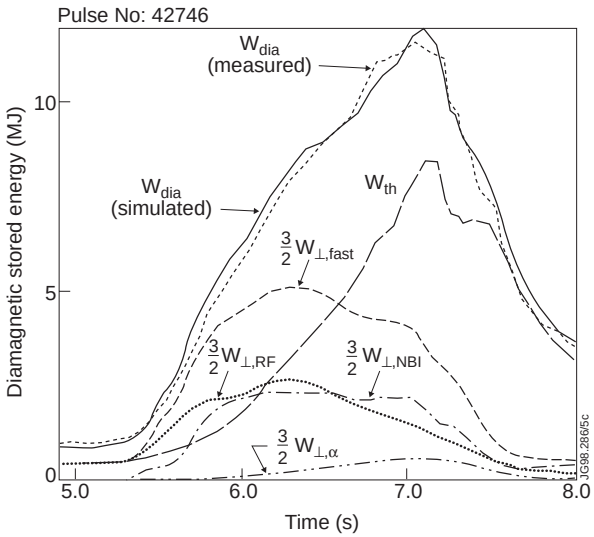

Fig. 7. TRANSP code modelling of the diamagnetic energy contents for deuterium-tritium pulse B, comparing the measured and simulated total diamagnetic energy contents (W_{dia}). Quantities: W_{th} ; thermal energy, $W_{\perp, RF}$; perpendicular component of the total RF fast ion energy, $W_{\perp, NBI}$; perpendicular component of the total NBI fast ion energy, $W_{\perp, \alpha}$; perpendicular component of the total fusion α-particle fast ion energy.

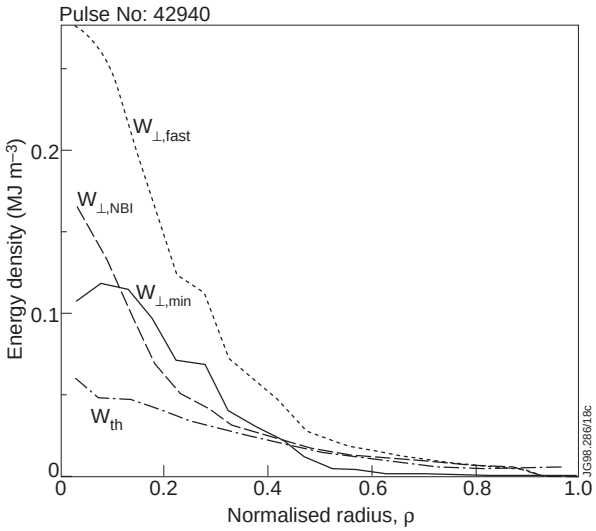

Fig. 8.Profiles of perpendicular energy density of the various plasma components at the time of the birth of the internal transport barrier for deuterium-tritium pulse No. 42940. W_{th}; thermal energy density, $W_{\perp,fast}$; perpendicular component of the total RF and NBI fast ion energy density, $W_{\perp,min}$; perpendicular component of the minority RF fast ion energy density, $W_{\perp,NBI}$; perpendicular component of the NBI fast ion energy density.

3. ICRF HEATING

3.1 ICRF Power Absorption

Central ICRF heating with $\pi/2$ phasing and frequency f = 51.2 MHz ($\omega = 2\omega_{cH} = 2\omega_{cD}$) was applied in pulse A (No. 40554). The RF power absorbed by the various species is shown in Fig. 9. In this calculation the bounce-averaged TRANSP Fokker-Planck model 2 (see Appendix) was used, which included the computation of the RF power damped on the injected deuterium ions at second harmonic resonance, $\omega = 2\omega_{cD}$, and the resultant distortion of the beam distribution due to this interaction. The split of the damped RF fast wave power between deuterium (P_D) and hydrogen (P_H) ions depends on the concentration of minority particles: $\eta = n_H / (n_H + n_D)$ in the central resonance layer and is given by the approximate relation [14]

$$\frac{P_D}{P_H} \propto \frac{\beta_D}{\eta} \qquad (1)$$

where β_D is the beta value of the deuterium ions. Thus, for a given minority concentration, the fast wave power damped on the ions increases in proportion to the core ion pressure. In the modelling, the calculated value of diamagnetic stored energy, W_{dia}, is largely insensitive to the assumed value of η, but the calculated D-D neutron rate, R_{NT}, is sensitive to this parameter [15, 16]. Both PION and TRANSP models are able to obtain good agreement between the calculated and measured D-D neutron rate, R_{NT}, assuming a fixed concentration of η = 3 % in pulse A. For reference, the effect of assuming a lower value η = 1.6 % in pulse A is also shown in Fig. 9.

Reducing the minority concentration lowers the total RF power absorbed on the minority ions and increases the power absorbed on the deuterium ions, by approximately 1 MW. With η = 1.6 %, the total predicted D-D neutron emission rate from the plasma increased by 8%, which lies just within the measurement error band.

To compare the RF code modelling, we have checked the TRANSP ICRF results with the independent PION ICRF code for the RF heating conditions of pulse A; the results are shown in Table III. The agreement between the two codes is reasonable, when one takes into consideration the fact that different equilibria (EFIT, in the case of PION) were used to map the plasma profiles on to the flux surface geometry.

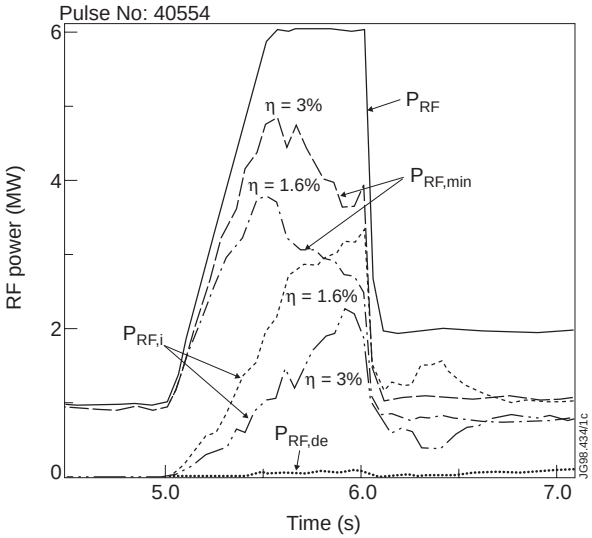

Fig. 9.RF power absorbed by the various species for pure deuterium pulse A. The traces are: total coupled RF power (P_{RF}), power absorbed by minority H ions ($P_{RF,min}$), RF power absorbed directly by D ions and RF power absorbed directly by thermal electrons ($P_{RF,de}$). Two cases are shown with assumed hydrogen minority concentrations of 3% and 1.6%.

TABLE III. Comparison of the PION and TRANSP RF code calculations of the RF power absorbed by different species for the pure deuterium optimised shear pulse A (No. 40554). The assumed hydrogen minority concentration was h = $n_H / (n_H + n_D)$ = 3 %

time	t = 5.95 s		t = 7.4 s	
Total Coupled RF power, P_{RF}	6.1 MW		2.0 MW	
	PION	TRANSP	PION	TRANSP
RF power absorbed by minority ions, $P_{RF,min}$	4.3 MW	4.1 MW	1.3 MW	1.1 MW
RF power absorbed directly by deuterons, $P_{RF,D}$	1.6 MW	1.9 MW	0.5 MW	0.8 MW
RF power absorbed directly by electrons, $P_{RF,de}$	0.2 MW	0.1 MW	0.2 MW	0.1 MW
Ratio: $P_{RF,D}$ / P_{RF}	27 %	30 %	23 %	38 %

As the coupled RF power, P_{RF}, is ramped up (from t = 5 s to 5.5 s), the power absorption (Fig. 9) takes place predominantly on the hydrogen minority ions. At t ~ 5.5 s, with the formation of an internal transport barrier and the build-up of energetic injected deuterium ion density, the central pressure of deuterium ions, $\beta_D(0)$ increases to a level where $2\omega_{cD}$ damping ($P_{RF,i}$) in the hot core becomes significant with respect to the local ion energy balance and comparable with the minority damping ($P_{RF,min}$). Of the RF power coupled to the deuterium, most went to

the injected beam ions having energies E > 3/2 T_i, and only a relatively small amount to the thermal deuterons with energies E < 3/2 T_i. The profile of the average energy of the NBI deuterons, $<E_{NBI}>$, perturbed by the RF interaction, is shown in Fig. 10; for comparison, the results of the Monte-Carlo NBI model are included to show the average energy of the unperturbed beam ions. The RF interaction increases the average energy of the NBI deuterons by typically a few tens of keV in the central part of the plasma $\rho < 0.25$. Independent PION calculations give a similar conclusion. The relatively modest increase in $<E_{NBI}>$ is insufficiently large to produce a strong deuterium tail (which could have enhanced the D-D beam-thermal fusion rate in the plasma centre [16], and led to data inconsistencies). The perturbed deuterium population still has an average energy lying significantly below the critical energy [17] in the plasma ($E_{crit}(0)$ ~ 190 keV in the example shown). The ratio of NBI ion to electron heating power is therefore not strongly affected by the RF interaction and still remains weighted strongly towards ion heating.

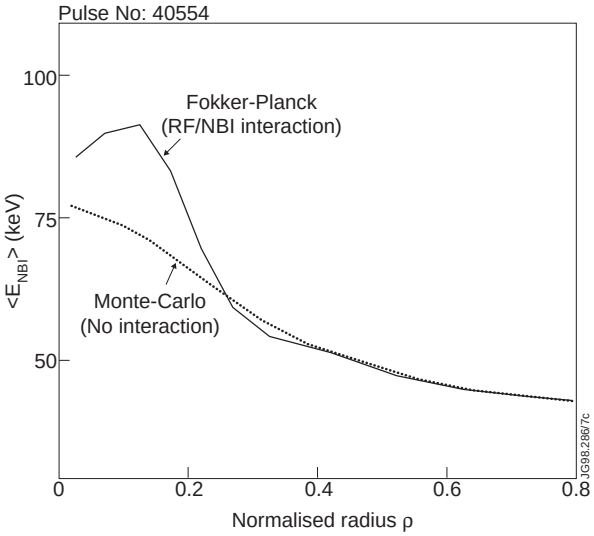

Fig. 10.Profile of the average energy of the NBI deuterons, $<E_{NBI}>$, perturbed by the RF interaction (TRANSP model 2), compared with the results of the unperturbed Monte-Carlo description (TRANSP model 1).

3.2 Power Deposition Profiles

The profiles of total ion and electron heating rate are given by sums of the direct heating rates (defined above), and the redistributed powers transferred by the minority ions to the plasma ions ($P_{RF,min,i}$) and electrons ($P_{RF,min,e}$) respectively. For the electrons, we therefore have: $P_{RF,e} = P_{RF,de} + P_{RF,min,e}$, and for the ions: $P_{RF,i} = P_{RF,D} + P_{RF,min,i}$. The volume-integrated power deposition profiles from both NBI and ICRH are shown in Fig. 11 at a time just before the step-down in the RF power. In the central region $\rho \leq 0.3$ the RF ion heating was comparable with that of NBI, despite the difference in applied powers (P_{RF} = 6 MW, P_{NBI} = 18.6 MW). This is a result of the strongly peaked RF power deposition.

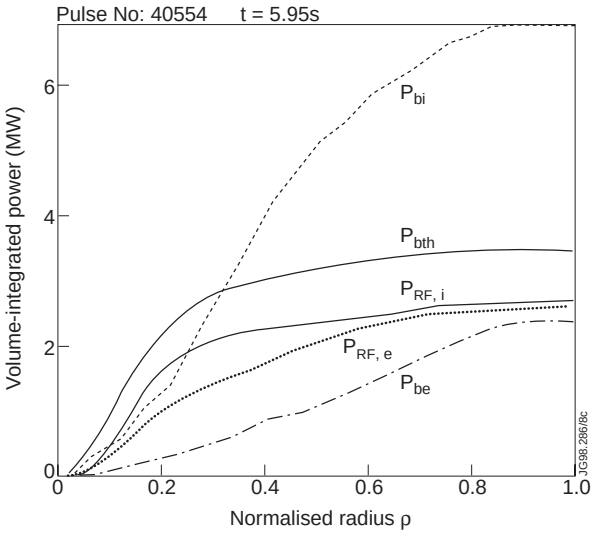

Fig. 11.Volume-integrated profiles of power deposited on the ions and the electrons from both NBI and ICRH for pure deuterium pulse A: P_{bi}; NBI ion heating power, P_{bth}; thermalised NBI heating power (see text), P_{be}; NBI electron heating power, $P_{RF,i}$; ICRF ion heating power, $P_{RF,e}$; ICRF electron heating power. The total input powers were: P_{RF} = 6 MW, P_{NBI} = 18.6 MW.

3.3 Plasma Response to the ICRF Power Step-Down

The RF power was stepped-down in discharge A (Fig. 2) at t = 6 s in order to avoid the high central plasma pressure gradients which were found to be unstable, both experimentally (sometimes resulting in disruption), and by MHD modelling [18]. At the peak performance times, the peaking of the pressure profile of these optimised shear plasmas is limited by pressure-driven ideal kink modes. In the highest performing cases, if the RF power is not stepped down, the MHD stability limit can be exceeded and disruption results. However, if the RF power is reduced to too low a value or switched off entirely, the L-mode edge plasma can be lost prematurely and an early H-mode transition is provoked.

In the example pulse A, the RF power was stepped down from 6 MW to 2 MW. The sudden step allows us to analyse the RF ion heating in some detail and correlate it with plasma parameters. In effect, one can think of this as a half-cycle of an RF modulation experiment. A clear response in the ion temperatures in the central region, can be seen before and after the power step in Fig. 3. After the step-down in the coupled RF power, the central ion temperature promptly decreased - from 27 keV to 23 keV - in a time of about 500 ms - reflecting the drop in central RF ion heating. This effect can be seen inside the region $\rho < 0.3$. TRANSP calculations predict pproximately 75% of the ICRH ion heating power in the discharge to be deposited inside the volume enclosed by $\rho = 0.25$. To analyse the response, we consider the time behaviour of the core ion energy content (W_i), obtained by volume-integration of the plasma ion energy density out to radius $\rho = 0.25$. The ion energy balance in this region is given by

$$\frac{d}{dt} W_i = P_{RF,i} + P_{NBI,i} - \frac{W_i}{\tau_i} \qquad (2)$$

where the time derivative of the core ion energy content is shown in Fig. 12, the first two terms on the right hand side of Eq. 2 are the heating powers to the ions from ICRH ($P_{RF,i}$) and NBI ($P_{NBI,i}$), and τ_i is the ion energy confinement time. We consider two times: t_1 = 6 s, just at the ICRH power stepdown and t_2 = 6.3 s, after the ICRH stepdown and at a time when the time derivative of the core ion energy content is relatively lower and deduce the change, $\Delta P_{RF,i} = P_{RF,i}(t = t_2) - P_{RF,i}(t = t_1)$ in the ICRH ion heating power at the step-down time. From TRANSP results we find $\tau_i \approx 0.3$ s in this time interval. Also, during this time interval we note that the ion thermal diffusivity in this region remains close to the standard neo-classical level (Fig. 13). At the two times (t_1 , t_2) the corresponding quantities on the right hand side of Eq. 2 are: $P_{NBI,i}$ = (2.8, 4.5) MW, W_i = (0.85, 1.32) MW respectively. We obtain $\Delta P_{RF,i}$ = 2.1 MW, with an estimated error of approximately 20%. This result, which is obtained for the core region defined above, can be compared with the total change in the RF ion heating power in the plasma at the stepdown time calculated using TRANSP (Fig. 9). This is $\Delta P_{RF,i}$ = 2.3 MW assuming a minority concentration of η = 1.6%, and is $\Delta P_{RF,i}$ = 1.75 MW assuming a minority concentration of η = 3.0%. We conclude that, at the step-down time of the ICRH, approximately half of the power coupled to the plasma is damped on the deuterium ions.

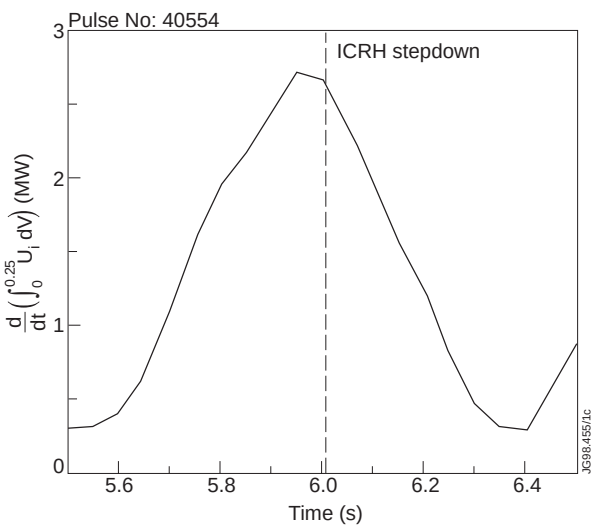

Fig. 12.Plot of the rate of change of the thermal ion density in the core region of pulse A (volume integrated out to ρ = 0.25) before and after the step-down of the ICRH power. A correlated response in this quantity can clearly be seen.

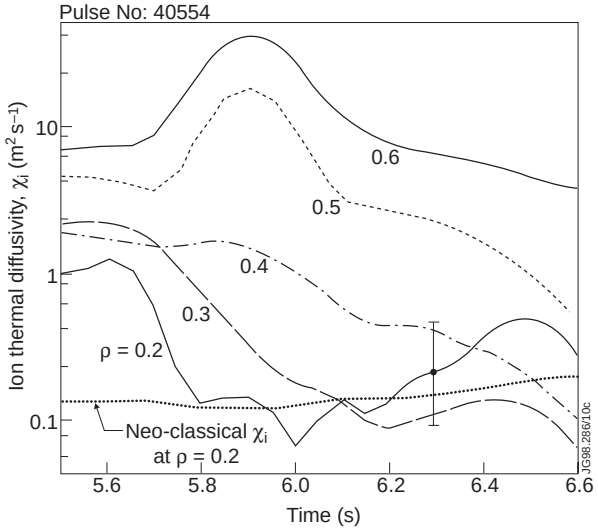

Fig. 13.Plot of the evolution of the ion thermal diffusivity, χ_i , at various radii for pure deuterium pulse A also showing the standard neo-classical level at ρ = 0.2. A typical error bar from TRANSP analysis is shown at this radius.

3.4 Comparison of Internal Transport Barriers with Stepped-Down ICRH and with Stepped-Down NBI

In experiments where we have attempted to maintain the fusion neutron production rate, we have used real-time control, to feedback on the heating waveforms using the neutron production rate as the control signal. We have successfully performed experiments in pure deuterium where both the ICRH and the NBI waveforms were separately under active control. In each case, one of the additional heating systems was stepped-down to maintain a preset fusion neutron production rate whilst keeping the other auxiliary power source fixed. These experiments give some indication on the relative heating efficiencies of the RF and NBI methods.

Overview waveforms of two such discharges with combined RF and NBI are shown in Fig. 14 where we compare two deuterium discharges: pulse ”A1” - No. 40210 with the NBI power stepped down, and pulse ”B1” - No. 40215 with the ICRH power stepped down. Both pulses had toroidal field B_T = 3.4 T and, although the current ramp waveforms were slightly different, each reached a plasma current of 3 MA at t = 6.5 s, during the internal transport barrier phase. In pulse B1 the heating waveforms are applied 0.5 s later than in pulse A1. The internal transport barriers form at: t = 5.6 s (case A1) and at t = 6.1 s (case B1). At these times the calculated q-profiles are both flat in the centre with the calculated location of the q = 2 surfaces appearing at radii $\rho \sim 0.46$ (case A1) and $\rho \sim 0.57$ (case B1). Each plasma remains in the L-mode until 6.83 s (case A1) and until 6.87 s (case B1). The high performance phases of both discharges are terminated by large ELMs at time t = 7.1 s.

In Fig. 14, the traces for pulse B1 have been plotted 0.5 s earlier for comparison and show that the fusion neutron rate in case A1 æAs held at a steady level $R_{NT} \sim 3.4 \times 10^{16}$ s^{-1} during the time period 6.5 s - 7.1 s when the NBI power had been stepped down from 17.1 MW to 10.2 MW

but the coupled RF power remained constant at the 6.1 MW level. The fusion reactivity is maintained even though the NBI power had been reduced below the level where internal transport barriers have not been observed in JET. Further experiments are needed to determine the role played by any hysteresis effect connected with a conceivably larger NBI power required to form the internal transport barrier than to maintain it. During the NBI step-down phase, the energy slowing-down time of the full energy NBI ions is 30 ms - 50 ms. PION calculations for these discharges show that NBI ions in the centre are accelerated to higher average energies ($<E_{NBI}> \approx 150$ keV) by the RF in pulse A1 than is the case in pulse B1 ($<E_{NBI}> \approx 100$ keV). Fig. 14 shows similar central plasma density evolution in both pulses. The ion temperatures, from crystal X-ray measurements at major radius R ≈ 3.4 m, are shown in Fig. 14. Both discharges reach near-central ion temperatures of 25 keV at about 0.4 s after internal transport barrier formation. In pulse A1, the higher level of RF power allows near-central ion temperatures of up to 27 keV to be maintained until $t \sim 7.1$ s, despite the step-down of the NBI power. The central electron temperatures are similar in both pulses up to time 1.8 s after the application of the main heating power, reaching $T_e(0) = 14$ keV at that time. With the later increase of the NBI power in pulse A1, $T_e(0)$ further increases to 15 keV at $t = 7.1$ s. A summary of the heating data is given in Table IV.

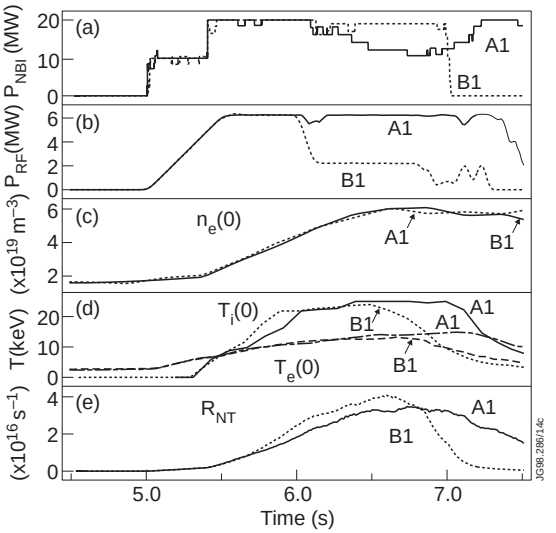

Fig. 14.Overview waveforms of two pure deuterium B_T = 3.4 T discharges: pulse "A1" - No. 40210 with the NBI power stepped down, and pulse "B1" - No. 40215 with the ICRH power stepped down. The traces for pulse B1 have been plotted 0.5 s earlier for comparison. Traces: (a) NBI powers, (b) ICRH powers, (c) central electron densities, $n_e(0)$; (d) central ion and electron temperatures, $T_i(0)$ and $T_e(0)$; (e) total neutron emission rates. Pulse A1 shows the fusion neutron production rate held at a steady level of $R_{NT} \sim 3.4 \times 10^{16}$ s^{-1}

Table IV also shows TRANSP model 1 analysis results of the breakdown of the volume-integrated ion heating powers delivered to the central region $\rho < 0.25$. We note the similarity between the total ion heating power, $P_{i,tot} = P_{NBI,i} + P_{RF,i}$, in both cases A1 and B1 (respectively 4.9 MW and 5.2 MW). In pulse A1, some 33 % of the total ion heating power in the inner region comes from RF. The relatively high direct ion heating efficiency of RF in the plasma centre is due, partly, to the narrow heating deposition region, partly to the low minority concentration and partly to the formation of the high β_i core. Comparing the central RF ion heating (region $\rho <$ 0.25) of A1 with B1, we find an increase of 0.8 MW of power for an overall increase of 4.1 MW of coupled ICRH power (implying an efficiency of 20 %). For comparison, we find an increase of 1.1 MW of NBI ion heating in the central region $\rho < 0.25$ for a total increase of 7.0 MW of injected NBI power (implying an efficiency of 16 %). PION calculations give similar results.

*TABLE IV. Values of heating powers during the ITB phases (*t = 6.8 s*). Pulse A1: No. 40210 with NBI power stepped down; pulse B1: No. 40215 with the ICRH power stepped down.*

	Pulse A1	Pulse B1
Total Input Power, P_{TOT}	18.3 MW	20.5 MW
D Beam Power, P_{NBI}	10.2 MW	17.1 MW
Coupled RF Power, P_{RF}	6.1 MW	2.0 MW
Total RF power to ions, $P_{RF,i}$ ($\rho < 0.25$)	1.6 MW	0.8 MW
RF power absorbed by minority ions, $P_{RF,min}$ ($\rho < 0.25$)	2.1 MW	0.6 MW
NBI ion heating power, $P_{NBI,\,i}$ ($\rho < 0.25$)	3.3 MW	4.4 MW
Total ion Heating Power, $P_{i,tot}$ ($\rho < 0.25$)	4.9 MW	5.2 MW
Ratio: $P_{RF,i} / P_{i,tot}$ ($\rho < 0.25$)	33 %	15 %

With the more peaked ion heating profile in the case where the NBI power was stepped down (pulse A1), we expect the profile of neutron emission to be more peaked. The neutron emission profiles from the neutron collimator diagnostic show full-widths at half-maxima (FWHM), equivalent to FWHM = 0.64 m and FWHM = 0.77 m at the position of the centre of the plasma, for cases A1 and B1 respectively. These values are consistent with an increase in the neutron emission profile peaking factor of ~ 20%. However, at the times of the peak total neutron emission in the two discharges, the calculated radius of the $q = 2$ surface was ~ 10% larger in pulse B1 than in A1. Therefore, given that we commonly observe the radius of the internal transport barrier to follow the calculated radius of the $q = 2$ surface during the L-mode phase of the discharge, it is likely that at least some of the pressure peaking effect is due to the difference in the position of the $q = 2$ surfaces between the two discharges. This implies that the central resonance and coupling of the RF to the plasma ions increases the peaking factor of the neutron profile by ~ 10 %. This conclusion is also supported by TRANSP and PION reconstructions. The plasma thermal pressure profiles (Fig. 15) are also more peaked in case A1 at $t = 1.8$ s after the application of the main heating power; the fractions of the plasma current carried by the bootstrap and the beam-driven currents are 31 % and 9 % respectively in case A1 and 25 % and 15 % in case B1. For case A1, we attribute the lower beam-driven current fraction to the reduced beam power and the higher bootstrap fraction to the more peaked plasma pressure profile.

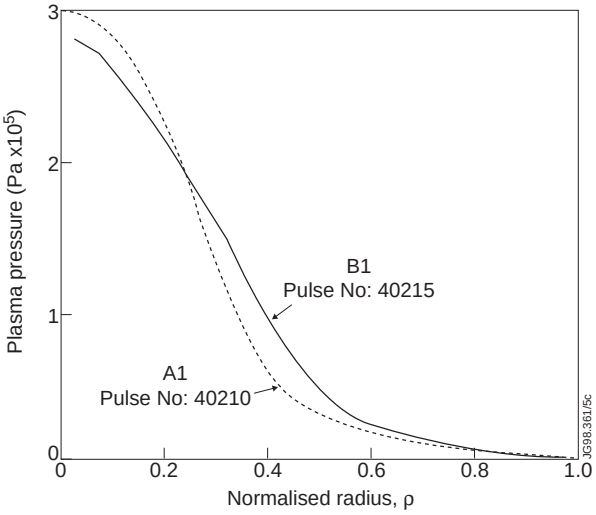

Fig. 15.Thermal plasma pressure profiles for pulses A1 and B1 at the time of peak fusion performance.

4. DISCUSSION

As we have seen, ICRH was used extensively, and in combination with NBI, to produce high performance optimised shear plasmas on JET, with internal transport barriers both pure deuterium and deuterium-tritium discharges. There still remain many unanswered questions concerning the physics of internal transport barriers. In this discussion we will concentrate on the ion internal transport barrier - the "standard case" - since the available diagnostic data is consistent and well documented. We consider two distinct phases of the plasma evolution: the plasma conditions prevailing at the time of the formation of the internal transport barrier, and the conditions which occur as the internal transport barrier evolves. ICRH plays a key role in both of these phases.

4.1 Conditions at the Barrier Formation Time

Our experiments show the importance of obtaining appropriate physical conditions in the plasma core at the time of barrier formation if high quality internal transport barriers are to be produced. First, the current density profile is important - the calculated evolution of the q(r) profile indicates the necessary presence of the $q = 2$ surface in the plasma with $q(0) = 1.5 \pm 0.5$ [19]. The magnetic shear is low and, on the basis of the available experimental data, the existence of a central region of weak negative shear is likely. If the main heating is applied too early or too late with respect to these conditions then either the barriers do not form at all or they are of poorer quality. The addition of ICRH to NBI, during the early main heating phase, is instrumental in producing internal transport barriers promptly and reproducibly. A strongly peaked pressure profile at the time of the internal transport barrier formation is observed. This gives rise to a steep pressure gradient in the low-shear region as well as a large Shafranov shift of the magnetic axis. The pressure in the plasma centre at this time is dominated by fast ions, being split approximately equally between injected beam ions in the 100 keV energy range and ICRH minority ions in the range of a few MeV. As the internal transport barrier evolves and the plasma density increases, the fraction of the plasma stored energy in the fast ion tail decreases. At the time that the ITB is triggered, the energetic minority ions have large drift orbits; the maximum radial excursion of these is given approximately by

$$r_{max} = R_0 (2.9 \rho_L q / R_0)^{2/3} \qquad (3)$$

[20] where ρ_L is the ion Larmor radius, and the major radius of the JET tokamak is $R_0 = 2.97$ m. At the time of the birth of the internal transport barrier, $q \approx 2$ near the resonance location and we calculate the maximum radial excursions of the energetic ICRH minority ion drift orbits to be typically $r_{max} \approx 0.6$ m - 0.7 m in these high performance discharges. The minority particle energy is calculated to be in the range 1 MeV - 3 MeV in the ICRH deposition region. The maximum radial excursions of the fast ion orbits lie just outside the $q = 2$ surface and the trapped energetic ions precess around the torus to form a fast ion current. The direction of the fast ion current density enhances the local current density and gives rise to a central flattening of the q(r)

profile. This effect [21] has been used to explain the stabilisation of MHD sawteeth in ICRH discharges with $q(0) \approx 1$, but, in the present context, may also play a role in helping to establish a suitable low shear region in the centre of the plasma to trigger the barrier. Indeed, as we have noted from the experiments, the combined application of ICRH with NBI results in the prompt formation of internal transport barriers. In addition, we note that the phasing of the ICRH antennas was different in pulse A (phase $+\pi/2$) than in pulse B (toroidal dipole phase). Nevertheless, the above conclusions apply.

4.2 The Growth of the Barrier and the Transition to ICRF Ion Heating

About 0.5 s after the application of the main NBI heating power, the injected co-beam-driven current reaches a maximum value of ~ 30 % of the total current and has a broad profile. The RF power damped resonantly on the injected beam ions has, by this time, increased to a level of ~ 1 MW which is absorbed preferentially, near the position of the harmonic resonances of the NBI species, in the centre of the plasma. This power absorbed by the injected beam ions increases their average perpendicular energy, increasing the fraction of them which are trapped in the toroidal field. Once trapped, these RF accelerated ions can no longer participate in the circulating beam-driven current and therefore, overall, there will be a net reduction of the beam-driven current source near the centre of the plasma. With co-injection, as in our experiments, this effect will tend to flatten the current density profile and tend to reinforce further the low shear region in the centre of the plasma.

As the central density of plasma and injected particles builds up, the beam-driven current is reduced in magnitude. However the central ion pressure increases on a timescale of ~ 1 s with the central region of improved confinement expanding with a radial velocity of about 0.5 m s^{-1} (Fig. 1). The magnitude of the bootstrap current fraction increases at this time. Throughout this period the RF damping on the injected ions increases until, after about 1 s after the application of the main heating, the injected ions absorb approximately half of the coupled RF power. The average perpendicular energy of the injected ions is increased by not more than a few tens of keV and still lies significantly below the critical energy of the plasma. The ratio of ion-to-electron heating efficiency of the beam particles is not strongly affected by the RF interaction and one can consider the RF power absorption on the beam ions to add to the ion heating power of the beams in the plasma core.

5. CONCLUSIONS

We have described recent experiments in the JET tokamak in which high fusion performance plasmas with low central magnetic shear have been produced with both pure deuterium and deuterium-tritium mixtures. A number of other tokamak devices have previously reported the formation of internal transport barriers using NBI auxilliary heating alone. In the work presented here, we have exploited a unique feature of the JET device in the optimised shear regime, the ability to heat efficiently the plasma core using ICRH, in addition to NBI. The improved core

performance occurs when an internal transport barrier forms, reducing the ion thermal diffusion losses in the central region of the plasma column down to values close to the standard neo-classical level.

ICRH performs three key roles in these discharges. Firstly, in the preheating phase, at a coupled power level of ~ 1 MW, ICRH heats thermal electrons efficiently up to temperatures of $T_e(0) \sim 4$ keV - 5 keV, and delays the penetration of the plasma current to the core during the ramp-up phase. Secondly, at the critical time of the birth of the internal transport barrier, the ICRH and NBI powers are both increased, forming a plasma whose energy content is dominated by energetic particles producing steep pressure gradients near the centre of the plasma. Approximately half of the plasma pressure comes from hydrogen minority ions having energies in the MeV range and these particles have maximum drift orbital radii of $\rho \sim 0.5$. Thirdly, once the internal transport barrier has formed and the central ion pressure begins to increase, the ICRF power begins to couple strongly to the ion component, supplementing the central ion heating ($\rho < 0.25$) and helping to maintain a steep ion pressure gradient at approximately half radius. During this phase, the calculated equilibrium shows the formation of a low central magnetic shear target plasma with $q(0) \approx 1.5 \pm 0.5$ and the rational q=2 surface close to the radius of the expanding internal transport barrier. In experiments where the ICRF power was kept constant and the NBI power stepped-down, the fusion reactivity was maintained even though the NBI power had been reduced below the power level at which it is difficult to form internal transport barriers in the present JET configuration. There may, in addition, be a hysteresis effect in the sense that a larger NBI power might be needed to form the internal transport barrier than to maintain it. Further experiments are needed to investigate this possibility.

The precessional motion of the ICRH fast ions can drive an off-axis current which tends to reduce the central magnetic shear. This effect may play a role in helping to establish the internal transport barrier. When ICRH is resonantly absorbed on the injected NBI ions in the centre of the plasma their perpendicular energy is increased, the ions become trapped in the toroidal field, and can no longer contribute to the beam-driven current. The effect of this tends also to reduce the central magnetic shear. Both of these specific ICRH effects are additive: they both tend to raise $q(0)$.

The experiments and analysis presented above have shown the beneficial effects of using ICRH in the development of high fusion performance JET plasmas with internal transport barriers and low central magnetic shear. With the ability to control the power deposition in localised and predetermined regions and to couple power to the plasma ions efficiently we plan to exploit further this technique to optimise plasma performance.

ACKNOWLEDGEMENTS

It is a pleasure for authors to acknowledge the contributions of Task Force P and the specific assistance of D.C.McCune and R.V.Budny from PPPL for their help in using the TRANSP code and of B.Lloyd, C.Warwick and C.Hunt from the Task agreement with the UKAEA.

APPENDIX: MODELLING AND ANALYSIS

The JET optimised shear discharges presented above have been reconstructed with the TRANSP transport code [22, 23]. This has the advantage that all measured plasma quantities, both global and local, can be incorporated within a standard computational scheme and checked for self-consistency. This code contains a magnetic equilibrium solver, Monte-Carlo models for the neutral particles, the injected beam ions and the fusion ions that are tracked during their slowing-down history. In the TRANSP neutral beam description, once the injected beam ions have slowed down to energies $E < 1.5\ T_i$, they are counted as thermal ions and no longer as beam ions; in effect, providing a sink for the "thermalised" fast ions. This cutoff enables the beam and thermal ion model calculations to be separated; in effect, this implements the joint paradigms that the thermal ions form a plasma component with anomalous transport properties that can be investigated separately from the energetic ion population which exhibits neo-classical transport behaviour.

ICRF Models

We have analysed data and cross-compared results using three different ICRF heating models: the TRANSP model with a Monte-Carlo NBI package (model 1), the TRANSP model with a Fokker-Planck NBI package (model 2) and, separately, with the PION code [24, 25]. In the TRANSP context, the wave fields are computed in the up-down asymmetric magnetic geometry relevant to the JET divertor geometry.

With TRANSP model 1 (Monte-Carlo beam model), we can also make use of an ICRF heating model based on a 2D full-wave solver, SPRUCE [26], which uses a dielectric tensor expanded in Bessel functions allowing wave damping on high energy ions having significant finite Larmor radius. This RF code is coupled with a small banana-width approximation bounce-averaged Fokker-Planck description, FPPRF [14], of the minority fast ion distribution which includes direct (second harmonic) damping on bulk ions as well as transit-time magnetic-pumping (TTMP) and Landau damping on thermal electrons. The effect of the second harmonic interaction of ICRF with energetic beam ions is also modelled and the RF power damped on energetic NBI deuterium or tritium beam ions computed. However, the NBI distribution remains unaffected by the damped RF power in this choice of model.

Alternatively, in the TRANSP context, for a description of the RF / NBI interaction process we can use a bounce-averaged Fokker-Planck description of the beam distribution which includes a quasi-linear RF operator (model 2). Here the ICRF treatment is similar to the above except that any RF power damped on the NBI injected ions can modify the NBI distribution function, causing the ions to diffuse up or down in energy. Because of the "thermalization" criterion in TRANSP (that is, beam ions with $E < 1.5\ T_i$ being treated as thermal), once the energetic ions diffuse below this boundary, they can no longer be accelerated above it by the RF to populate the tail. This will lead to unphysically enhanced thermalization.

The PION code is a time-dependent code which calculates the ICRF power deposition and the velocity distribution function(s) of the resonating ions. In the power deposition calculation the launched wave is Fourier decomposed in the toroidal direction. The power deposition is then calculated for each toroidal mode number according to the model described in Refs [27, 28]. Owing mainly to finite Larmor radius effects, the absorption strength depends on the distribution function of the resonating ions. In order to take this into account, the dielectric tensor components used in the power deposition calculation are updated, using results from the Fokker-Planck calculation, at the beginning of each time step according to the procedure described in Ref. [16]. The distribution function of the resonating ions is calculated with a time-dependent 1D Fokker-Planck equation [24]. Effects due to finite orbit widths are taken into account by assuming that the fast ions have turning points close to the cyclotron resonance (i.e. where $\omega \sim n\omega_{ci}$) and then averaging the collision coefficients over the resulting orbits. Furthermore, the averaged square parallel velocity, which is used to determine the Doppler broadening of the cyclotron resonance in the power deposition calculation, is obtained from an *ad hoc* formula derived in Ref. [29]. In order to take into account the the influence of the beam particles on the ICRF power deposition, NBI source terms have been included [21] in PION.

REFERENCES

[1] Tubbing B. et al, Nuclear Fusion **31** (1991), 839.

[2] Hugon, M. et al., Nuclear Fusion **32** (1992), 33.

[3] Levington, F.M. et al., Phys. Rev. Lett. **75** (1995), 4417.

[4] Strait, E.J. et al., Phys. Rev. Lett. **75** (1995), 4421.

[5] Fujita,T. et al., Plasma Physics and Controlled Nuclear Fusion Research, Proc. 16th Int. Conf., Montreal, 1996, IAEA-CN-64/A1-4.

[6] Gormezano, C., et al. 1997 Plasma Physics and Controlled Nuclear Fusion Research, Proc. 16th Int. Conf., Montreal, 1996, IAEA-CN-64/A5-5.

[7] Sips, A.C.C. et al., Proc. 24th European Physical Society Conference on Controlled Fusion and Plasma Physics, Berchtesgaden, Germany, 1997.

[8] Söldner, F.X., et al. Topical Paper. Proc. 24th European Physical Society Conference on Controlled Fusion and Plasma Physics, Berchtesgaden, Germany, 1997.

[9] Sips, A.C.C. et al., Plasma Phys. and Controlled Fusion, **40** (1998) 1171

[10] Cottrell, G.A., et al. Plasma Phys. and Controlled Fusion, to be published (1998)

[11] Gormezano, C. et al. Phys. Rev. Lett. **80** (1998), 5544.

[12] Righi, E. et al. submitted Nuclear Fusion (1998)

[13] Litaudon, X. et al., Plasma Phys. and Controlled Fusion, to be published (1998)

[14] Hammett, G.W., "Fast Ion Studies of Ion Cyclotron Heating in PLT Tokamak", Ph.D Thesis, Princeton, USA, (1986).

[15] Mantsinen M., et al., Plasma Phys. and Controlled Fusion, to be published (1998)

[16] Mantsinen M., et al., Proc. 24th European Physical Society Conference on Controlled Fusion and Plasma Physics, Berchtesgaden, Germany, **21A(1)** 137 (1997).
[17] Stix, T.H., *Waves in Plasmas* American Institute of Physics, ISBN 0-88318-859-7 (1992)
[18] Huysmans, G.T.A. et al., Proc. 24th European Physical Society Conference on Controlled Fusion and Plasma Physics, Berchtesgaden, Germany, **21A(1)** 21 (1997).
[19] Baranov, Y. et al. Nuclear Fusion, in preparation (1998)
[20] Stringer, T.E., Plasma Phys. **16** (1974) 651.
[21] Core W.G.F. and Cottrell, G.A., Nuclear Fusion **32** (9) (1992) 1637.
[22] Goldston, R.J. et al. 1981 J.Comput.Phys. **43** 61.
[23] Goldston, R.J. in Basic Processes of Toroidal Fusion Plasmas. 1986 Proc. Course and Workshop Varenna, 1985. Vol I, CEC Brussels 165.
[24] Eriksson, L.-G., Hellsten, T., and Willén, U., Nuclear Fusion **33** 1037 (1993).
[25] Eriksson, L.-G. and Hellsten, T., Physica Scripta **55** 70 (1995)
[26] Evrard, M. and Ongena, J., American Institute of Physics Conference Proceedings, "RF Power in Plasmas", 11th Topical Conference, Palm Springs, USA, 235, 1995.
[27] Hellsten, T. and Villard, L., Nuclear Fusion **28** 285 (1988)
[28] Hellsten, T. and Eriksson, L.-G., Nuclear Fusion **29** 2165 (1989)
[29] Andersson, D. *et al*., Plasma Physics and Controlled Fusion **29** 891 (1987)